EUROPEAN ORGANIZATION FOR NUCLEAR RESEARCH

CERN-EP/2003-017
March 31, 2003

Performance of the NOMAD-STAR detector.

G. Barichello[a], A. Cervera–Villanueva[b,c], D.C. Daniels[d], E. do Couto e Silva[b,1], M. Ellis[e,2], D. Ferrère[b,3], J.J. Gómez–Cadenas[b,c], C. Gössling[f], M. Gouanère[g], J.A. Hernando[c,4], W. Huta[b], J. Kokkonen[b,5], V.E. Kuznetsov[b,h,6], L. Linssen[b], B. Lisowski[f,7], J. Long[b], A. Lupi[i,8], Ö. Runolfsson[b], B. Schmidt[f,9], F.J.P. Soler[b,e,10] D. Steele[j], M. Stipčević[k], G. Vidal-Sitjes[b], M. Veltri[i].

Abstract

The NOMAD-STAR detector is a silicon vertex detector installed in the NOMAD spectrometer at the CERN SPS neutrino beam. It consists of four layers of a passive boron carbide target with a total mass of 45 kg and five layers of 600 single sided silicon microstrip detectors covering a total area of 1.14 m^2. About 11,500 ν_μ charged current interactions were reconstructed in the fiducial volume of NOMAD-STAR from the neutrino run in 1998. The potential use of silicon detectors for $\nu_\mu(\nu_e) \leftrightarrow \nu_\tau$ oscillations depends on the observation of the τ candidates by the experimental signature of a large impact parameter, in the case of the one prong decay of the τ, or a double vertex, in the case of the three prong decay. The main aim of NOMAD-STAR is to measure the impact parameter and vertex distributions of charged current interactions, which constitute the main backgrounds for the oscillation signals, to understand the significance of a potential signal in a future experiment. The present paper describes the experience gained in the operation of this silicon vertex detector, and the performance achieved with it.

PACS: 13.15.+g; 14.60.Lm; 14.60.Pq; 29.40.Gx; 29.40.Wk
Keywords Neutrino physics; Silicon microstrip detectors.

a. University of Padova, Padova, Italy.
b. CERN, Geneva, Switzerland.
c. IFIC, Universidad de Valencia, Spain.
d. Harvard University, Cambridge, MA, USA.
e. University of Sydney, Sydney, Australia.
f. Dortmund University, Dortmund, Germany.
g. LAPP, Annecy, France.
h. Joint Institute for Nuclear Research, Dubna, Russia.
i. University of Urbino, Urbino, and INFN, Florence, Italy.
j. University of Lausanne, Lausanne, Switzerland.
k. Rudjer Bošković Institute, Zagreb, Croatia.

Submitted to Nuclear Instrumentation and Methods.

[1] Now at Stanford Linear Accelerator Center, USA.
[2] Now at Rutherford Appleton Laboratory, UK.
[3] Now at the Université de Genève, Geneva, Switzerland.
[4] Now at Universidad de Santiago de Compostela, Spain.
[5] Now at Helsinki Institute of Physics, Finland
[6] Now at Fermi National Laboratory, USA.
[7] On leave of absence from Institute of Electron Technology, Warsaw, Poland.
[8] Now at University of Glasgow, Glasgow, UK.
[9] Now at CERN, Geneva, Switzerland.
[10] Now at the University of Glasgow and Rutherford Appleton Laboratory.

1 Introduction

There now exists strong evidence for neutrino oscillations from atmospheric neutrinos [1, 2, 3, 4], which can be interpreted as $\nu_\mu \leftrightarrow \nu_\tau$ oscillations, and from solar neutrinos [5, 6, 7, 8, 9, 10, 11], with the $\nu_e \leftrightarrow \nu_\mu$ oscillation hypothesis as the most plausible [12]. These results are to be verified by long baseline accelerator and reactor experiments [13, 14, 15, 16, 17]. In addition, two experiments at the short baseline CERN SPS beam, CHORUS and NOMAD [18, 19], have been searching for the exclusive $\nu_\mu(\nu_e) \leftrightarrow \nu_\tau$ mode and have found no evidence for oscillations, setting limits in the cosmologically relevant high Δm^2 region of phase-space [20, 21]. CHORUS distinguishes the ν_τ from the background of ν_μ interactions by identifying the kink from the short-lived τ decay inside an emulsion target (a topological search), while NOMAD identifies the τ decay by its kinematical signature inside a light drift chamber target. For a recent and comprehensive review of neutrino oscillations, see [22].

Proposals have been made for a future $\nu_\mu(\nu_e) \leftrightarrow \nu_\tau$ appearance experiment containing a large surface silicon tracker with a passive target [23] or with an emulsion target [24, 25]. The signature of a potential ν_τ interaction needed to separate it from the large background of ν_μ charged current (CC) events relies on the relatively long lifetime of the τ candidate ($c\tau = 86.93$ μm), which results in an impact parameter distribution (see Fig 1) that is wider on average than the impact parameter distribution of ν_μ events. The impact parameter (d) is defined as the projected signed distance of the closest approach of the μ^- from a ν_μ CC interaction (or the decay track from the one-prong decay of a τ in the case of a ν_τ CC interaction) to the vertex produced by the remaining hadronic jet. In the case of a three prong decay of the τ (for example, a decay to three pions), the most significant signature for the selection of the τ candidates is the observation of a double vertex consistent with the τ lifetime.

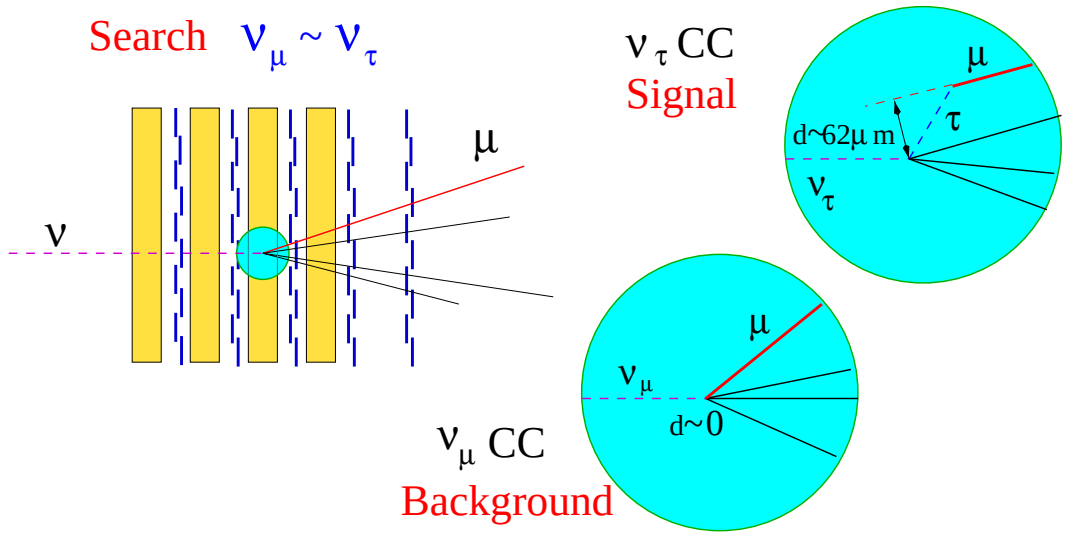

Figure 1: Definition of the impact parameter.

The fully electronic signal from the silicon detector is particularly well suited for a neutrino factory environment [26, 27, 28] because of the high event rate. In addition, other short-lived particles, such as charm particles from neutrino interactions, could be identified.

To understand the capabilities of a silicon detector in a neutrino experiment, a prototype of an instrumented Silicon TARget (NOMAD–STAR) was installed in NOMAD at the CERN SPS at the beginning of 1997 and it was operational until the end of the NOMAD 1998 run. NOMAD–STAR was installed upstream of the first NOMAD drift chamber [19, 29] (see Fig. 2).

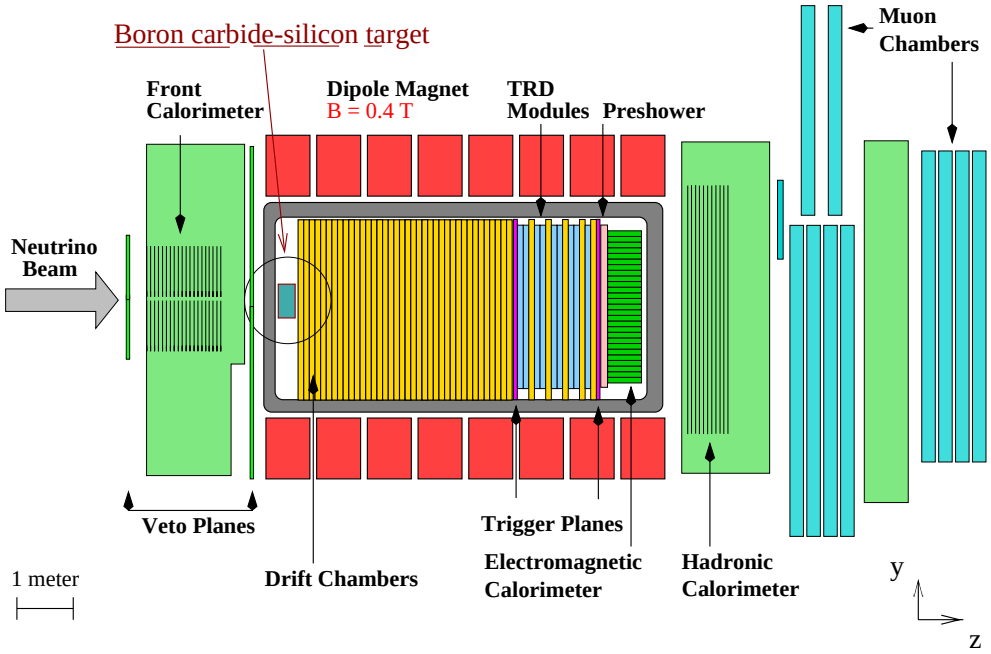

Figure 2: The NOMAD detector with the Silicon TARget (NOMAD–STAR).

NOMAD–STAR consists of four layers of boron carbide (B_4C) with a total mass of 45 kg, interleaved with five layers of single–sided silicon microstrip detectors[11] (see Fig. 3). Boron carbide provides the best compromise between high density ($\rho = 2.49$ g/cm^3) and long radiation length ($X_0 = 21.7$ cm) for low Z materials.

The five layers of silicon detectors have an active surface of 1.14 m^2. Each layer consists of 10 overlapping ladders, with 12 silicon microstrip detectors per ladder, read out by low–noise VA1 chips[12]. Each of the ladders are 72 cm long, and, to our knowledge, are the longest silicon ladders built to date. There are 5 chips to a ladder and there are two ladders for each repeater board connected to the mother-board. The detectors are single–sided strip detectors with thickness 300 μm, dimensions 33.5 mm $\times$ 59.9 mm, and with strip and readout pitches of 25 μm and 50 μm, respectively. There are 641 possible readout strips but only 640 of them are actually read out. That constitutes 6,400 channels per layer, which is a total of 32,000 readout channels for the whole detector. The readout strips are parallel to the NOMAD magnetic field (x axis) and provide information on the y projection of the track. The detectors are AC coupled, FOXFET biased [31] and passivated with silicon oxide. The performance of the silicon ladders has been described in [32], where a beam of pions with momenta higher than 100 GeV/c was used to determine that the point resolution of a ladder of 12 detectors is about 5 μm. A detailed description of the NOMAD–STAR detector and its construction can be found in reference [33].

The present paper describes the experience gained in the operation of NOMAD-STAR and the measured performance of the detector. Section 2 describes the data collected during the operation of NOMAD-STAR, section 3 describes the pedestal and noise performance of the silicon ladders, section 4 shows the optimisation of the hit-finding efficiency for each of the NOMAD-STAR ladders, section 5

[11] Manufactured by Hamamatsu Photonics, Japan.
[12] A commercial version of the Viking chip [30]

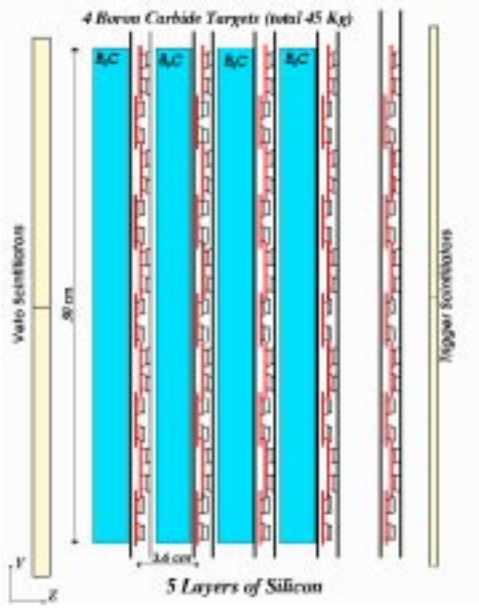

Figure 3: Side view of the silicon target, showing the four boron carbide and five silicon layers (comprising ten staggered ladders each), along with the veto and trigger scintillators. The neutrino beam enters from the left. Each silicon ladder is represented by the silicon sensor and the four carbon fibre rods that comprise the supporting backbone, all enclosed in the aluminium casing.

describes the track reconstruction procedures and the results obtained, while sections 6 and 7 will show the vertex resolution and final impact parameter distribution achieved with NOMAD-STAR.

2 Data

2.1 Monte Carlo

2.1.1 Geometry

The detector components of NOMAD–STAR falling in the fiducial volume are implemented in detail in the GEANT 3.21 [34] description of the detector. See Fig. 3 for a diagram, with a full description of the detector in Ref. [33]. The 600 silicon detectors are positioned individually in the volume, as are the carbon fibre pieces and insulating kapton layer (on which the silicon detectors rest) comprising the ladder support. Aluminium covers, placed in front and behind each silicon layer, have also been implemented and so have the scintillators for the veto and trigger system.

The individual elements are all placed in their nominal positions relative to each other, except for the silicon detectors, whose positions are smeared according to distributions obtained from the detector alignment procedure [35, 36]. The position of NOMAD–STAR with respect to the NOMAD frame-of-reference has been determined by an optical survey after the installation of NOMAD–STAR in NOMAD [33].

2.1.2 Hit reconstruction and charge sharing model

Only those hits passing through the active areas of the silicon detectors are recorded, after which the detector response is simulated in a process called the "digitisation". In the case of NOMAD–STAR,

the charge recorded by the analog-to-digital converters (ADCs) for each strip is simulated. The charge is expressed in ADC units, with one ADC unit corresponding to approximately 250 e^-.

The digitisation algorithm is based on data obtained from test-beam experiments of silicon module prototypes [32] and from muons passing through NOMAD–STAR during the data-taking. The total charge deposited by a charged particle traversing the detector follows a Landau distribution with a peak-value of approximately 100 ADC counts above pedestal. The charge is shared amongst several readout strips, taking into account the interstrip and backplane capacitances according to "Algorithm C" of Ref. [32]. Instead of a strip retaining all the charge deposited on it, it was found that 17% of the charge is passed onto each neighbouring strip with 5% of this charge being lost to the backplane through capacitive coupling[13]. It is assumed that for the readout strips the capacitive coupling to the amplifiers is much larger than that to the backplane and that the floating strips retain no charge in the end. In addition, the strips are smeared with the noise, which has a Gaussian distribution, centered at zero and assumed to have a standard deviation of 6 ADC counts. The common-mode noise (see sub-section 3.2) is not simulated.

In the first step of the charge sharing model, the total deposited charge is shared between the nearest readout and floating strips, the charge split in proportion to the distance of the hit from the strips. In the next step, 70 % of the charge on the readout strip is read out, while 15 % goes to each of the neighbouring floating strips (in addition to the charge retained by the floating strip). Of the charge on a floating strip, 5 % of the charge passes to the backplane and is lost, with the rest of the charge distributed evenly between the two neighbouring readout strips (47.5% each strip). This step is repeated until the contribution to the readout charge is negligible, in practice eight times. The total charge which is read out is the sum of the readout charges for that strip for the eight steps.

2.1.3 Beam Monte Carlo

The NOMAD neutrino beam simulation package NUBEAM [37] was used to determine the flux and average energies of the four species of neutrinos passing through NOMAD–STAR. These are ν_μ , $\overline{\nu_\mu}$, ν_e and $\overline{\nu_e}$, with a negligible contribution from ν_τ [38, 39]. The beam simulation is based on GEANT 3.21 [34] with the hadronic component reweighted by the stand-alone implementation of FLUKA [40] corrected by results from the SPY experiment [41]. The detector was placed deliberately below the centre point of the NOMAD drift chambers so that the beam would pass through the centre of NOMAD–STAR (the neutrino beam forms an angle of 42 mrad with respect to the horizontal z-axis of NOMAD). The concentration and average energy of the neutrino species are shown in table 1 and the predicted spectra in NOMAD–STAR are shown in Fig. 4.

Neutrino	Average Energy (GeV)	Concentration (%)
ν_μ	30.60	94.12
$\overline{\nu_\mu}$	19.83	5.02
ν_e	42.18	0.69
$\overline{\nu_e}$	31.11	0.17

Table 1: NUBEAM predictions for the NOMAD–STAR target.

2.1.4 Monte Carlo Statistics

The NUBEAM program described above is used to determine the beam spectra and composition to be used as an input for NEGLIB, the NOMAD event generator based on LEPTO 6.1 [42] and JETSET 7.4

[13] In Ref. [32] there is an error and ϵ and ϵ_b should be reversed. It should read $\epsilon = 0.172$ and $\epsilon_b = 0.052$

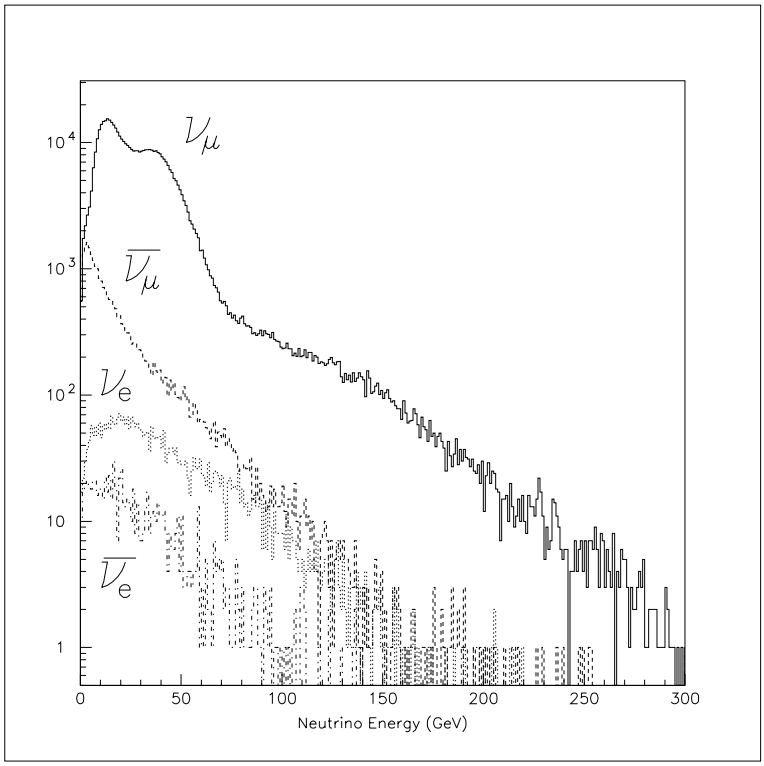

Figure 4: The neutrino spectra of ν_μ, $\overline{\nu_\mu}$, ν_e and $\overline{\nu_e}$ at NOMAD–STAR as predicted by NUBEAM.

[43] that simulates the neutrino events in the NOMAD–STAR volume. The NOMAD-STAR GEANT simulation is included in the overall GENOM program that is the GEANT description of the whole NOMAD detector. A total of 69,000 ν_μ charged current (CC) events were generated and these will be used for comparisons to data throughout this paper.

2.2 Data acquired

2.2.1 Running conditions

NOMAD-STAR took data continuously during the 1997 and 1998 SPS neutrino runs at CERN. The trigger was formed by the logic condition $\overline{V_8} \times \overline{V_S} \times T_S \times T_1$, where $\overline{V_S}$ is the logical OR of signals from two scintillators in front of the target in anticoincidence, T_S is the OR from two scintillators downstream of the target, $\overline{V_8}$ is the signal from the central NOMAD veto also in anticoincidence and T_1 is the signal from the first of the two NOMAD trigger scintillator planes [33, 44]. A total of 13 CAEN VME V550 flash ADC modules, with 10 bit resolution, operating at 1 MHz clock rate, were used to read out the 32,000 strips. Each of the 25 ADC channels (2 channels per module) used serial multiplexing to read out its corresponding 1280 strips. The sensors had a 60 V reverse-bias voltage and these were read out by the VA1 chips with a shaping time of 3 μs. The ADC integration time was 1 μs, so each ADC read out all the channels in a time of 1.3 ms. The timing signals of the V550 modules were controlled by a CAEN V551B sequencer. The pedestals were calculated online prior to a data run and subsequently subtracted inside the ADC modules with the zeros suppressed. The data transfer from the 13 VME V550 modules to a central CPU took approximately 10 ms.

There were two neutrino spills in each 14.4 s SPS cycle. Each spill was approximately 5 ms wide, separated by a 2.4 s interval to allow for the 2.0 s spill used for the SPS test-beams (known as the "flat-top"). Since the NOMAD-STAR readout was so long, a special busy logic formed in a dedicated

electronics module was used to inhibit a second NOMAD–STAR trigger for each neutrino spill. During the normal neutrino running period, the trigger rate was measured to be $(0.33 \pm 0.07)/10^{13}$ protons on target (*pot*). The livetime is defined as the fraction of time that a NOMAD-STAR trigger is not inhibited by the busy signals when an actual $\overline{V_8} \times \overline{V_S} \times T_S \times T_1$ trigger fires. This was measured with dedicated scalers to be $(59 \pm 5)\%$. During the 1998 run, there were two periods when the SPS ran with negative particle focusing in the West Area Neutrino Facility (WANF), causing a predominantly $\overline{\nu_\mu}$ beam. The rate during these running periods was $(0.17 \pm 0.07)/10^{13}$ *pot* with a livetime of $(75 \pm 5)\%$. A timing problem of the trigger logic in 1997 also reduced the trigger rate for the standard positive focused ν_μ beam down to $(0.17 \pm 0.07)/10^{13}$ *pot* during the data taking of that year. An additional trigger made of the coincidence $V_8 \times V_S \times T_S \times T_1$ was also used to select muons passing through NOMAD–STAR during the SPS flat-top.

2.2.2 Event filter

As mentioned previously, a timing problem of the trigger logic in 1997 significantly reduced the rate of good events in the 1997 run. The relative timing of the coincidence signals for triggering was offset so there was only a small effective area of the trigger scintillators that remained active. Out of a total number of 98,858 NOMAD–STAR events triggered, only 998 events were good events in the NOMAD–STAR fiducial volume [45]. In addition, since the trigger was biased towards one edge of the fiducial volume it was difficult to obtain proper efficiency measurements. For this reason, this data sample will not be used any further.

The main data sample comes from the 1998 run. A total of 423,249 NOMAD–STAR triggers were recorded throughout the year. The great majority of these triggers are caused by interactions in the vicinity of the NOMAD–STAR volume (for example, the coil of the NOMAD magnet and in two additional targets made of aluminium and carbon situated beneath NOMAD–STAR). A filter was developed to pre-select valid NOMAD–STAR events. These were subdivided into three categories:

- NOMAD–STAR vertex events, where a primary vertex is reconstructed in the NOMAD–STAR volume from silicon hits (11,528 events);
- NOMAD–STAR track events, which are events that do not pass the NOMAD–STAR vertex criteria but have at least one reconstructed NOMAD–STAR track (29,442 events);
- DC vertex events, which are events that do not pass the two previous criteria but have a reconstructed vertex in the NOMAD–STAR fiducial volume from the reconstruction of drift chamber (DC) tracks (4,600 events). These vertices are due to tracks that have not triggered the NOMAD-STAR trigger scintillators (either escaping on the edges or due to scintillator inefficiencies) or to misreconstructed vertices from the DC into NOMAD–STAR.

From the Monte Carlo samples, it was shown that 100% of neutrino interactions in NOMAD–STAR that produce a valid NOMAD–STAR trigger were accepted by these three criteria. In practice, only the 11,528 events in the first category (NOMAD–STAR vertex events) are used for any analysis since silicon hits are needed to measure the performance of the NOMAD–STAR detector.

3 Pedestals and Noise

3.1 Pedestals

The numbering scheme for the NOMAD–STAR silicon layers adhered to in this paper will be the following. The layers are numbered 1-5 with layer 1 the furthest upstream and layer 5 next to the drift chambers. Each silicon layer contains 10 ladders, ladder 1 being the bottom-most ladder, and 5

electronics chips per ladder, chip 1 being the bottom-most. Although each chip has 128 channels, all the 640 channels on a ladder are numbered consecutively, again with channel 1 at the bottom.

The pedestals are the average values of the channels read out when there is no signal. This base-level on the channels is typically of the order of 200-400 ADC counts, depending on the channel. The pedestal file for a run is compiled using data from the previous run. The data is taken during the calibration cycle of the beam, i.e. during the approximately 12 s of no beam of the full 14.4 s cycle. Of the order of 10-20 calibration events are recorded using pulsed triggers during each calibration cycle. In order to make the pedestal file for the following run, 2600 pedestal calibration events are required.

The pedestal data is always stored in a database and then used by the V550 ADC to automatically subtract the pedestals from the stored signals. Therefore, the pedestal-subtracted data for each channel is centered around zero in the absence of signal. In addition, the data acquisition rejected information from channels in which the pedestal-subtracted ADC was exactly zero (zero-suppression). The pedestals are characteristic to each ladder and were found to be very stable. An example of the pedestals for a ladder is shown in Fig. 5.

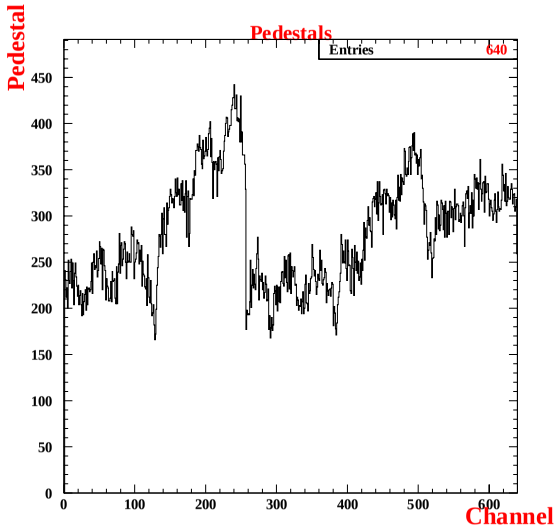

Figure 5: The pedestals (in ADC counts) for the 640 channels of ladder 1 on layer 1. A channel-by-channel approach is used and the pedestals are recalculated for every run.

3.2 Noise production

The noise is calculated independently from the procedure to calculate the pedestals. It is done off-line on a day-by-day basis using data from muon events in the SPS flat-top. The noise is defined as the RMS fluctuation of the read-out signal value around the base value, or pedestal, after common-mode noise (CMN) subtraction when there is no true signal. The noise is measured in units of ADC counts, with 1 ADC count corresponding to approximately 250 e^-.

For each event used to calculate the noise, the CMN is established first. The CMN is the average, or common, jump in the signal-level for all 128 channels on a chip for an event due to a common pick-up of noise.

The event-by-event CMN subtraction is performed according to the following procedure for each chip:

- the average pedestal-subtracted signal is calculated,

- the root-mean-square (RMS) deviation around the CMN for all channels on the chip is calculated,
- only those channels for which the RMS deviation around the CMN is between 0.9 and 25 ADC counts are selected,
- the CMN per chip is recalculated, further selecting only those channels which have a signal value within three times the RMS from the chip mean,
- the CMN value is subtracted from the read-out signal value for all channels on the chip.

Once the CMN subtraction has been performed, the RMS noise is calculated using muon events as a trigger. All strips for which the read-out value is not within three times the RMS are excluded. This is to avoid using real hits due to muons in the noise calculations.

The procedure outlined above results in day-by-day noise files for each of the 32,000 channels, with the number of muon events per day used for these calculations ranging from approximately one hundred to a few thousand. The full 1998 neutrino run consists of 171 days but there are 9 days in which there was either no data or insufficient data to make good noise files.

3.3 Noise behaviour

The noise behaviour of NOMAD–STAR throughout the 1998 data-taking period was studied extensively [46, 47]. The total sample consists of 162 daily noise files over the 171 day data-taking period. The noise was mainly studied at the chip level (128 channels) since it was impractical to study the 32,000 channels individually. The chip noise was defined as $\sqrt{\frac{1}{128}\sum_{i=1}^{128} N_i^2}$, where N_i is the noise of the ith strip on the chip.

Most chips exhibited a very stable noise rate of approximately 6 ADC counts throughout the year. An example is shown in Fig. 6, showing the day-by-day noise of the chips from a stable ladder (day 1 corresponds to 2 April and day 171 to 19 September 1998).

However, there were other chips that showed more unstable noise behaviour, characterised by periods in which the noise increased gradually from the base-level to level-out at a higher noise value. Abrupt resetting of the noise level would occur when the detector was switched off for a few days, for example in the case of scheduled service interventions in NOMAD. An example is shown in Fig. 7. It should be noted that at approximately day 140, the detector is only switched off for 7 hours and the noise-level is not completely reset. This suggests that the detector resets gradually after being switched off. All unstable chips showed the same general behaviour and three distinct periods can be identified. In April (up to day 25), the noise was fairly stable with only a slight increase, in May up to mid-June (days 28-70) there was a period of steady increase and from mid-June (day 70) the increase in the noise is more pronounced, reaching a plateau within 20 days. One can also conclude that the changes from day-to-day are small and that daily noise files are adequate.

It is interesting to note that all the chips from a ladder and individual channels in a chip showed mutually similar behaviour, apart from small peaks and ripples. This justifies the approach that the general noise behaviour can be determined at the ladder level. However, ladders connected to the same repeater card did not necessarily show similar behaviour. In summary, chips on 13 ladders (about a quarter of the total) showed the unstable noise behaviour clearly, although chips on up to a dozen further ladders showed some signs of this.

The distribution of RMS noise for the 250 chips during the whole data taking run in 1998 is shown in Fig. 8 (left). The noise distribution is centered around 6 ADC counts with the full-width-half maximum value at approximately 1 count. This corresponds to about 1500 e^-. Since the thickness of the fully depleted region of the silicon detector is 300 μm, one expects a signal of 25,000 e^-. Hence, the measured or signal-to-noise ratio (S/N) is approximately 17:1, in agreement with previous estimates [32] and measurements in the laboratory [33]. However, 49 chips showed this unstable behaviour, with

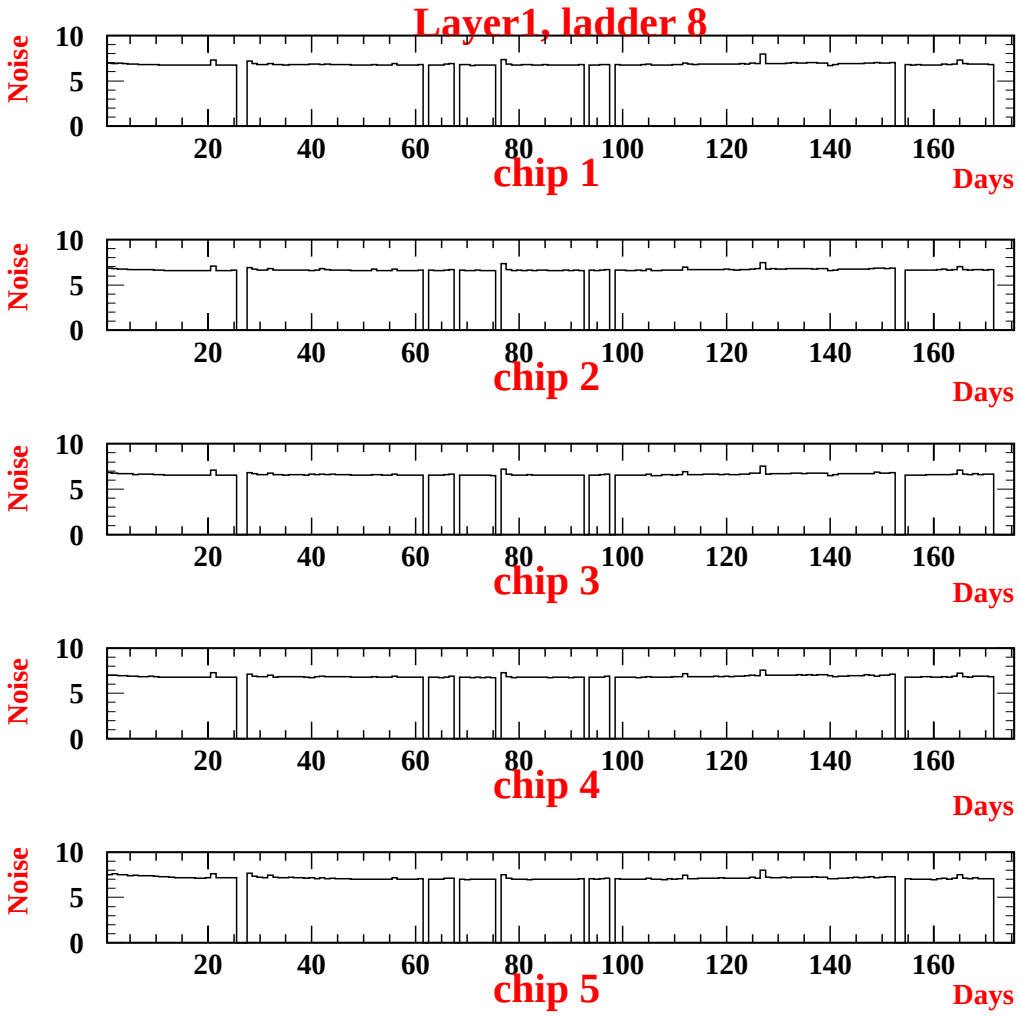

Figure 6: Chip noise evolution in time. The horizontal axis represents the days in the 1998 run from April to September 1998. The vertical axis shows the RMS ADC noise count for the chip. The gaps correspond to days with no data.

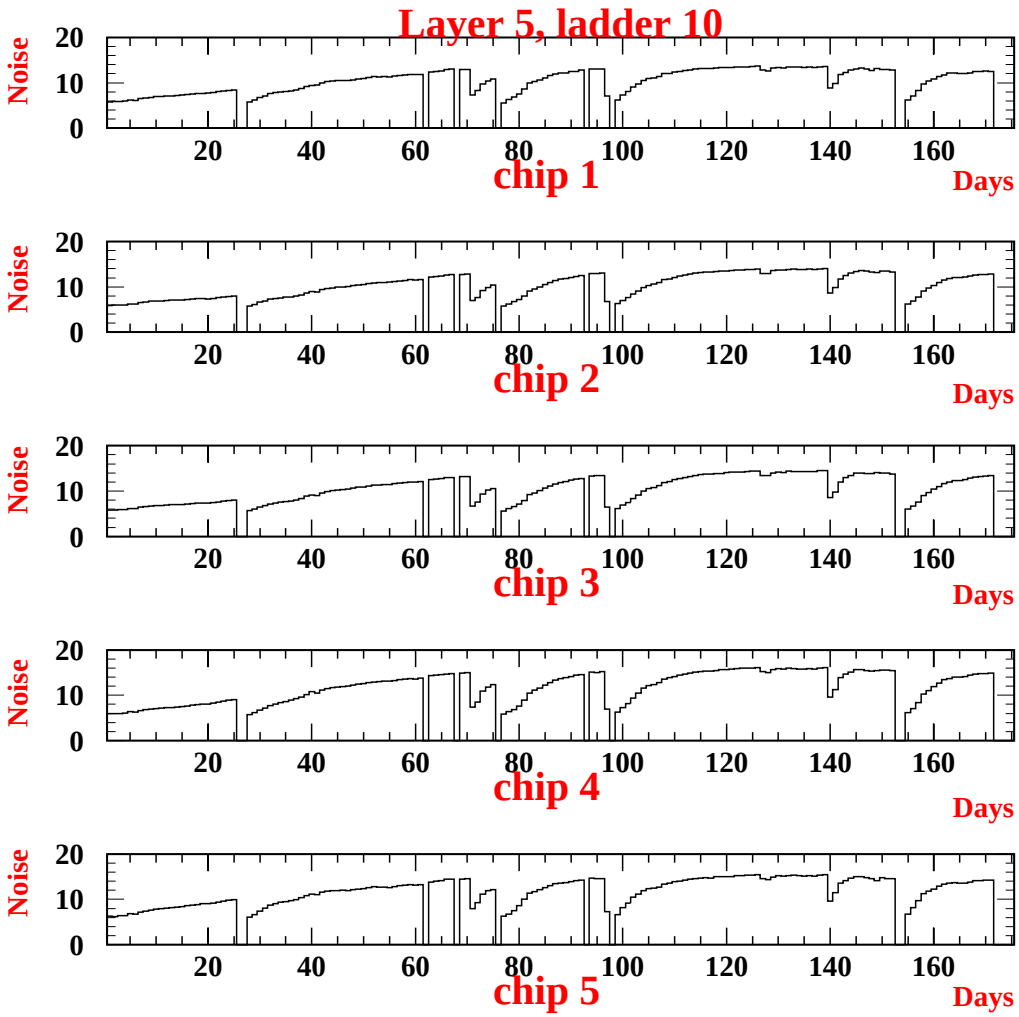

Figure 7: Noise evolution for unstable chips for April through to September 1998.The vertical axis shows the RMS ADC noise count for the chip. The gaps correspond to days with no data.

an average noise greater than 8 ADC counts (S/N less than 13:1). Finally, the ladder-by-ladder noise is shown in Fig. 8 (right) to identify which ladders have high noise. It should be noted that layers 3 and 4 in particular have high-noise ladders, along with ladder 10 of layer 5. One can also see in Fig. 11 the average Landau distribution of the signal (after some cluster selection cuts, see section 4.2), with a peak at 92 ADC counts, which corresponds to a S/N of 16:1.

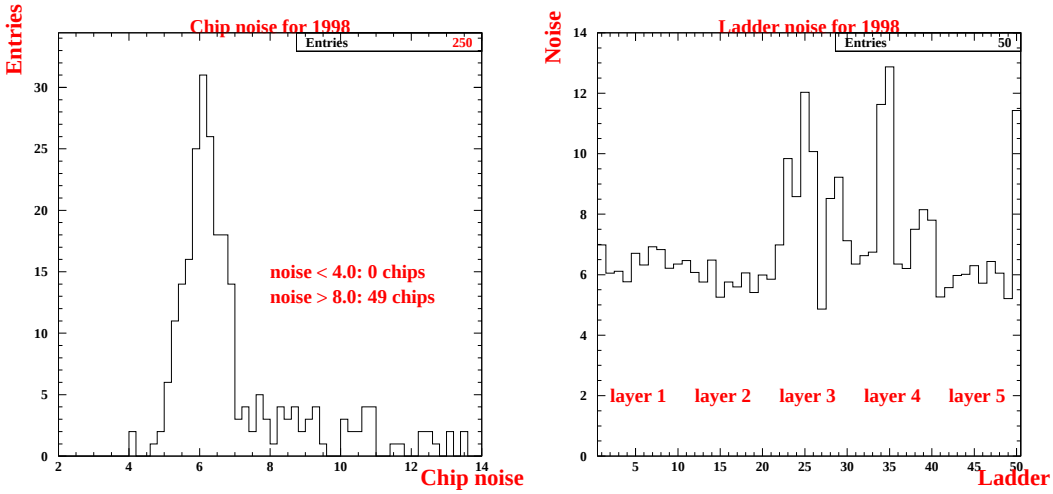

Figure 8: Left: The distribution of average chip noise for 1998. Right: The average noise for 1998 shown ladder-by-ladder.

4 Hit Efficiency

4.1 Hit-finding

When a charged particle traverses the detector, the charge is shared amongst neighbouring strips due to capacitive coupling, as described earlier [32]. The readout strip that has the highest charge is called the seed strip while collectively the strips sharing the charge are called the cluster. Hits are identified based on the following signal-to-noise ratio (S/N) criteria:

- a cut on the S/N of the seed strip: the seed cut,
- a cut on the S/N of the neighbouring strips: the neighbour cut,
- a cut on the sum of the S/N of the strips included in the cluster, according to $(S/N)_{cluster} = (S/N)_{seed} + \sum_i (S/N)_{seed-i} + \sum_i (S/N)_{seed+i}$: the cluster cut.

The following algorithm is used when forming clusters to identify hits:

- all strips with a S/N above the seed cut are sorted in order of decreasing S/N,
- seed strips are required to be separated by at least two strips; if not, seed strips with lower S/N are not considered,
- starting from the seed strip with the highest S/N, a maximum of three consecutive strips on either side of the seed strip are included in the cluster until a strip does not pass the neighbour cut or it has already been taken by another cluster,

- finally the cluster is required to pass the cluster cut.

The final hit position is determined by the "Algorithm C" model in [32], taking into account the interstrip and backplane capacitances.

4.2 Calculating the hit-finding efficiency

The efficiency studies are performed using reconstructed muon events. To ensure adequate statistics, the efficiencies are calculated ladder-by-ladder. As each ladder consists of 12 individual silicon detectors which are bonded together, there is a gap in the active region between each of these detectors. Therefore, for the purposes of the efficiency study, only tracks which pass through a fiducial active region of each layer are used. Hits placed 0.5 cm from the edge of the detectors were not considered for this study. The tracks are also required to pass through the same corresponding ladder of each layer, e.g. the 3rd ladder of each layer. This implies that the muon tracks should be straight. The relationship between the angle of muon tracks in NOMAD–STAR and the momentum of the muons is shown in [35, 36]. To avoid high-angle tracks and to minimise the multiple scattering angle, only muons above 10 GeV momentum are selected for the efficiency study.

The muon track is reconstructed such that a hit is required in each of the four equivalent ladders in the layers not under study. For example, if the 3rd ladder of the 1st layer is under study, a hit is required in the 3rd ladder of layers 2, 3, 4 and 5. The area within 1 mm of the extrapolated (or interpolated) hit position of the muon track to the ladder under study is considered for hits. The overall efficiency is defined as the ratio of the number of times at least one hit is found to the total number of muon tracks considered. For the single-hit efficiency, exactly one hit (or, equivalently, one cluster) is required within the 1 mm roadwidth. When considering single-hit efficiency, those cases which have two or more hits within the roadwidth are not allowed. This serves the purpose of limiting the number of times a so-called ghost hit is mistakenly used for efficiency calculations.

Initially, all the ladders were given the same seed (S/N $>$ 4.0), neighbour (S/N $>$ 0.5) and cluster (S/N $>$ 7.5) cuts, as discussed in [32]. However, due to differences in the noise response of individual ladders (see section 3) and possible differences in the gain, cuts were optimised for each individual ladder.

4.3 Hit-finding efficiency

The efficiency is maximised by optimising the S/N cuts as a function of ladder. This is done by first maximising the single-hit efficiency for the seed cut, while setting the neighbour cut to 0.5 and ignoring the cluster cut. So, for every ladder, the seed cut is optimised so that the efficiency to find exactly one strip passing the seed cut within the 1 mm roadwidth is maximised. Next, the seed cut and the fixed neighbour cut of 0.5 are retained and the efficiency is maximised by varying the cluster cut. This results in seed cuts for the ladders which vary from 3.4 to 4.4, with a median value of 3.9 while the cluster cut varies from 3.8 to 6.1, with a median value of 4.8. The seed and cluster cuts are shown by ladder in Fig. 9. The cluster cut of ladder 5, layer 2, is lower than the seed cut, a consequence of the optimisation algorithm, indicating that for this ladder the cluster cut plays no role. By comparing to section 3, one sees that there appears to be a weak inverse correlation between the ladder noise and seed cut.

The overall efficiency resulting from the optimised cuts is shown in Fig. 10 and in Table 2, along with the statistical error (depending on the number of muons traversing each ladder). Layers 2 and 3 attain a level of nearly 100%, with layer 1 at a slightly lower efficiency. The performance of the ladders in layers 4 and 5 is somewhat worse, even dropping below 95%. It is not surprising that layer 1 does not show optimum performance as this layer contains the ladders that had certain problems during construction (for example dead channels or larger leakage current). The poor performance of ladders 4 and 5 can be traced to calibration errors of the electronics, as discussed in the next section.

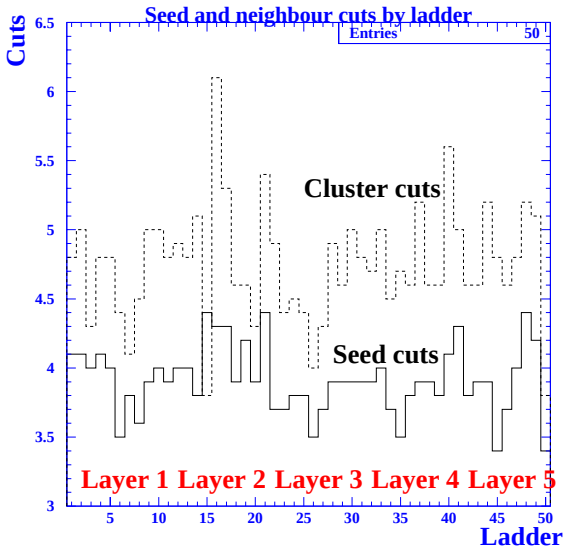

Figure 9: The seed and cluster cuts by ladder. The solid line corresponds to the seed cut and the dashed line to the cluster cut.

As a comparison, the overall efficiency is also shown in Fig. 10 with all ladders using fixed cuts of 4.0, 0.5 and 7.5, for the seed, neighbour and cluster cuts, respectively. The efficiencies are considerably lower, and more importantly, there is considerable fluctuation, justifying the approach of optimising the cuts ladder-by-ladder. No evidence was found for a change in efficiency as a function of time. These efficiencies are the final average efficiencies over the whole NOMAD-STAR data-taking period and supersedes the previous preliminary results over a limited period reported in [48].

ladder/layer	1	2	3	4	5
1	98.6±0.2	99.6±0.1	99.5±0.1	98.7±0.2	97.7±0.2
2	99.2±0.1	99.6±0.1	99.6±0.1	98.8±0.2	97.1±0.2
3	99.1±0.1	99.7±0.1	99.5±0.1	99.1±0.1	96.8±0.3
4	99.4±0.1	99.7±0.1	99.6±0.1	99.2±0.1	93.4±0.4
5	98.6±0.3	99.4±0.2	98.7±0.3	98.0±0.4	93.6±0.6
6	$100.0^{+0.00}_{-0.07}$	99.4±0.3	99.4±0.3	95.9±0.6	92.2±0.8
7	99.9±0.1	99.8±0.1	99.4±0.1	99.1±0.2	96.7±0.3
8	99.3±0.1	99.94±0.04	99.94±0.04	99.0±0.2	97.3±0.3
9	98.3±0.2	99.6±0.1	99.0±0.2	99.2±0.2	99.0±0.2
10	98.6±0.4	99.7±0.2	99.6±0.2	93.9±0.7	97.4±0.5

Table 2: The overall hit-finding efficiency (%) and statistical error for the ladders.

The effects of these cuts can be seen when silicon hits reconstructed from data and ν_μ CC Monte Carlo are compared. For the Monte Carlo samples the seed, neighbour and cluster S/N cut were 4.0, 1.0 and 6.0 respectively. A common set of S/N cuts had to be used in the ideal case of the Monte Carlo, while the data needed the optimised cuts to achieve the highest possible hit-finding efficiency. The total signal (in ADC counts) and the S/N for a cluster are shown in Fig. 11. There are more

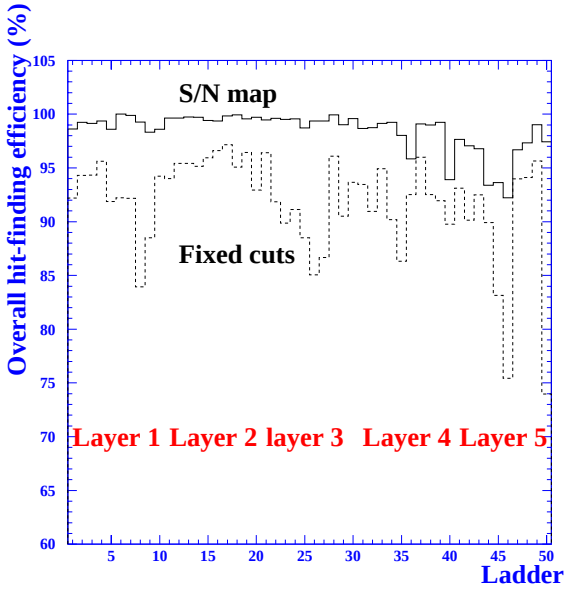

Figure 10: The overall hit-finding efficiency by ladder for optimised and fixed S/N cuts. The solid line corresponds to the optimised cuts and the dashed line to fixed cuts.

clusters with a low total signal and S/N in the data due to the lower seed and cluster S/N cuts and also due to the possible use of noisy strips to create a cluster.

4.4 Hit-finding efficiency in the laboratory

Layers 1 and 5 were investigated in the laboratory after the 1998 run to see whether the losses in efficiency were due to the ladders themselves or due to the electronics. The ladders were tested individually, sandwiched between a pair of scintillators for triggering, using a Ru-source. A hit in the ladder was recorded for a seed cut of 5.0, with no neighbour or cluster cuts used. The efficiency was defined as the ratio of the number of hits in the ladder to the total number of triggers.

The ladders were tested with the same repeater card as in NOMAD–STAR and also with one optimised in the laboratory. The repeater card contains the amplifying and shaping circuitry, although the pre-amplifiers are on the ladders themselves. The results are shown in Fig. 12.

For layer 1, the efficiencies with the optimised electronics are slightly better than with their own electronics. This suggests that a slight advantage could have been gained by fine-tuning the gain and shaping time of the electronics. However, as both sets of electronics give comparable results, yet some of the efficiencies are low, it is clear that part of the performance degradation is due to the ladders themselves. It should be noted that poor performance is shown for ladder 5 in the laboratory measurements. As this poor performance is not seen in the off-line efficiency studies, the low efficiency is presumed to be due to a failure of the ladder occuring after the 1998 run, for example due to mishandling of the ladder.

For layer 5 there is a dramatic drop in efficiency for ladders 5, 6 and 10 when using their own electronics compared to the optimised electronics. Further investigation of the settings of the corresponding repeater cards showed that they had been incorrectly calibrated. It should be noted that when using the optimised electronics with layer 5, the measured efficiencies (for a S/N cluster cut of 5.0) for Ru pulses are over 90%.

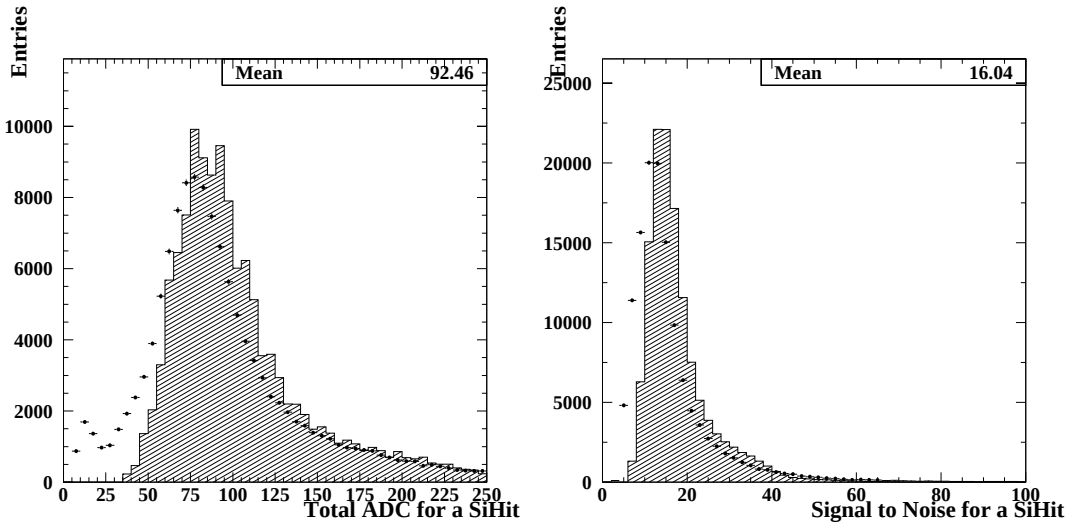

Figure 11: Left: Total ADC signal selected in a cluster by the S/N cuts. Right: Total signal to noise distribution in a cluster selected by the S/N cuts. The data points are overlayed on the ν_μ CC Monte Carlo histogram, which has been normalised to the data. The mean values correspond to the data.

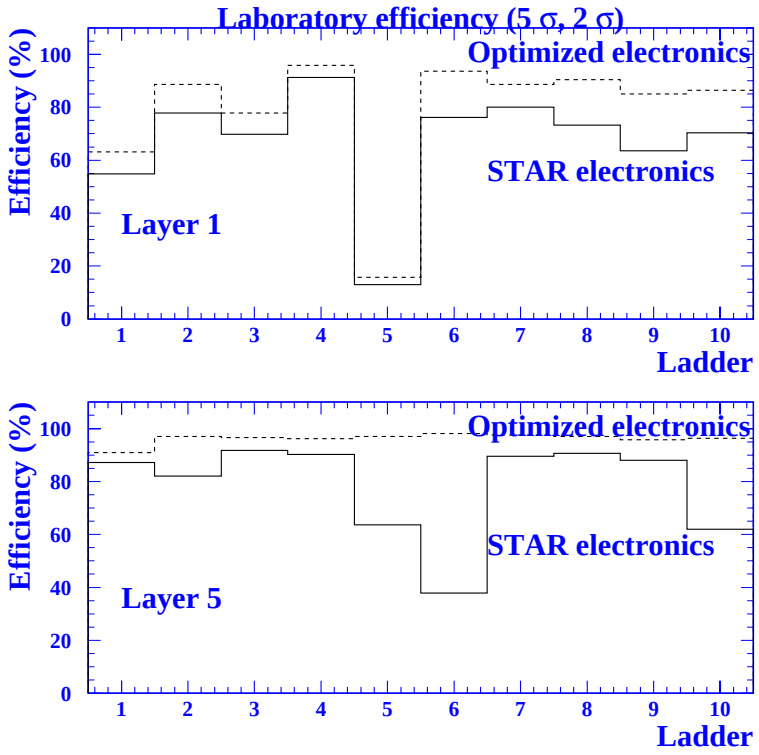

Figure 12: Ladder efficiencies in the laboratory for layers 1 and 5.

5 Track Reconstruction

Once the individual hits in NOMAD–STAR have been reconstructed, it is neccesary to identify which hits correspond to which track. Due to the lack of any information in the x-direction, it is necessary to extrapolate already reconstructed tracks in the drift chambers into NOMAD–STAR and use this information to both allocate hits to a given track and determine the optimum position of each hit. Once this information is obtained, the NOMAD–STAR hits can be fitted in the y-z plane to provide optimum track parameters inside the detector.

5.1 Pattern recognition

The pattern recognition process involves identifying which hits in NOMAD–STAR correspond to a given track in the drift chambers. In order to minimise incorrect associations, two cuts are implemented to select suitable drift chamber tracks (DcTracks). The DcTrack must have a reconstructed momentum of more than 150 MeV, and the most upstream hit of the track must have a z position of less than 100 cm (for comparison, NOMAD–STAR is fully contained between 5 and 20 cm in z).

For all DcTracks passing these cuts, an iterative procedure is followed:

- Each DcTrack is extrapolated to the downstream ladders of layer 5 (closest to the drift chambers) to check that the x position lies within the active volume of NOMAD–STAR. The extrapolated position in y is then tested against each hit (SiHit) in the corresponding NOMAD–STAR ladder.
- The difference in y divided by the approximate uncertainty due to multiple scattering (measured from the material the DcTrack traversed) is accumulated for each plausible combination of assigning hits to tracks. The combination with the lowest overall weighted difference is then chosen.
- The procedure is then repeated for the remaining ladders of layer 5, followed by each half of layer 4 and so on to layer 1.
- Once a single SiHit has been associated to a DcTrack, the position of the silicon strip that was hit can be determined more accurately by the knowledge of the individual silicon detector it traversed and the accurate alignment constants for that detector [35, 36]. The algorithm used to reconstruct the precise location of the hit was described in detail as "Algorithm C" in [32]. Up to eight strips are considered on each side of the seed strip and the charge collected on each is taken into account. The charge shared by the readout and floating strips as well as with the backplane is taken into account to determine the hit position.
- This position can be used as the starting point of the next extrapolation. In this manner, the accuracy of the hit assignment is not degraded by the existing material between layers 1 and 4. The extrapolation is improved further once 2 hits are associated to a DcTrack, since the two accurate positions in y and z are used in conjunction with the measurement of the momentum of the track from the drift chambers.
- In order to further minimise incorrect associations, the x position of the extrapolation of the DcTrack to the detector under consideration is used to determine if it is an active silicon region. Only if the x position corresponds to an active region of silicon is the association of a SiHit with that DcTrack allowed. If no hit is associated then a "hole" is defined for that layer. Once a track exceeds 1 unexplained hole, the extrapolation process for that track is stopped.

5.2 Reconstruction residuals

The reconstruction algorithm was described in detail in [36]. A Kalman filter algorithm [49] was used to perform the track and vertex reconstruction based on a cubic track model. The ladders of

NOMAD–STAR were aligned internally and with respect to the NOMAD drift chambers by using calibration muons available from the CERN SPS flat-top. The muons are reconstructed by using the Kalman filter and the alignment is performed by minimising the residuals for all the ladders. The residuals obtained after the alignment procedure were 9 μm for the ladders in the three inner layers (layers 2-4) and a value of 12 μm for the two outer layers (layers 1 and 5).

Fig. 13 shows the residuals for all hits in all tracks reconstructed by NOMAD–STAR. The data is represented by points with error bars, overlayed on ν_μ charged current Monte Carlo. The RMS of this distribution is 8.6 μm.

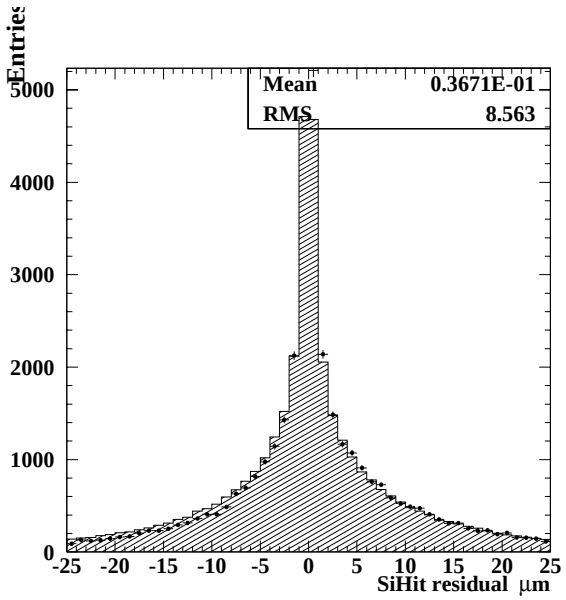

Figure 13: Distribution of residuals for all hits (μm).

6 Vertex resolution

6.1 Pattern recognition

The limitations of the 2 dimensional information recorded by NOMAD–STAR become evident during the vertex building and fitting stage. As each track is only recorded as the projection of the true track onto the y-z plane, it is not sufficient to look at crossing points of tracks to determine an estimate of the location of the neutrino interaction (primary vertex).

The procedure starts by finding ν_μ charged current (CC) events by searching for a muon candidate NOMAD–STAR track (SiTrack). If there exists a muon of the correct sign as identified by the muon chambers, then it is selected as a ν_μ CC event. If there is no such track, then the track of type "Unknown" (which is a track that is not identified as an electron, muon or pion by other NOMAD subdetectors [19]) with the correct sign and highest momentum is chosen.

This muon candidate is then tested against all other SiTracks in the event to find the crossing point in the y-z plane. If the crossing point is within the boundaries of NOMAD–STAR, then all other SiTracks are extrapolated to this position and the amount by which this extrapolation misses the crossing point is compared with a cut of 100 μm. The combination of muon and another track that allows the largest number of tracks to pass this cut is taken as the basis for building the primary vertex.

These tracks are fitted into a primary vertex using the vertex Kalman filter described in [36] and the remaining tracks are tested against the new position returned by the fit. Any more tracks which are now consistent with the new vertex position are added and the vertex is refitted.

6.2 Multiplicity and vertex position

For this comparison, the filtered sample of 11528 events from the 1998 data taking run are compared with the 62880 simulated ν_μ CC events passing through the filter.

There is a difference in the multiplicity distribution of the number of reconstructed tracks in NOMAD–STAR per event between data and Monte Carlo (Fig. 14). The Monte Carlo sample did not contain any quasi-elastic or resonance events (only deep inelastic scattering events) so the number of low multiplicty events is higher for the data. In addition, inefficiencies in the ladders might be reducing the hit track reconstruction efficiency with respect to the Monte Carlo, thereby increasing the excess of low multiplicity events in the data.

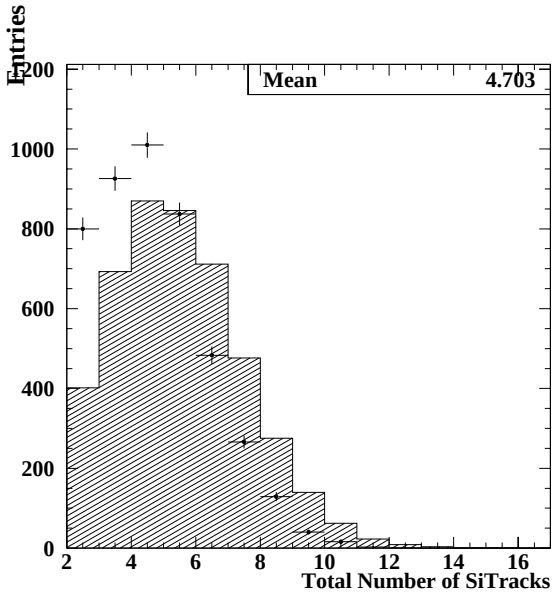

Figure 14: Distribution of the number of NOMAD–STAR tracks in the primary vertex for data (points) and for ν_μ CC Monte Carlo (histogram). Note the excess of events with 2 or 3 tracks in the data due to the absence of quasi-elastic and resonance events in the simulation. The mean number of tracks per event found in the data is 4.7.

The reconstructed x, y and z vertex positions are shown in Figs. 15 and 16. As NOMAD–STAR has no x information, the x vertex is determined exclusively from the drift chambers (DC). One can observe the vertices being reconstructed well within the NOMAD–STAR volume.

The distribution of the reconstructed z position (Fig. 16) of the primary vertex shows the structure of the NOMAD-STAR detector as shown in Fig. 3. The number of events in the layers closest to the DC is larger than those furthest away since the algorithm commences in the DC and extrapolates DC tracks into the NOMAD–STAR volume. The Monte Carlo only simulated primary neutrino interactions in the four blocks of B_4C, which is why there are very few reconstructed interactions in the gaps between the blocks. In the data, the silicon ladders, carbon fibre supports and aluminium covers have resulted in a small number of interactions between the passive targets. Imposing three tracks in the vertex improves the agreement between data and Monte Carlo, as shown in Fig. 16 (right) since it reduces

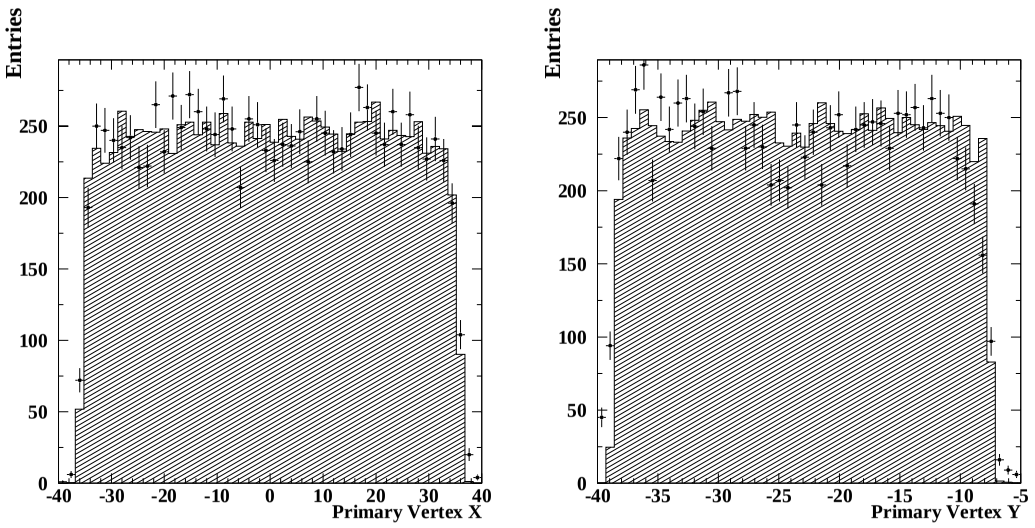

Figure 15: Distributions of the x (left) and y (right) positions (in cm) of the primary vertex.

the number of fake vertices. The remaining excess of data events in the regions between the B_4C plates is due to interactions in the carbon fibre supports, the aluminium plates supporting each layer and interactions in the silicon detectors themselves.

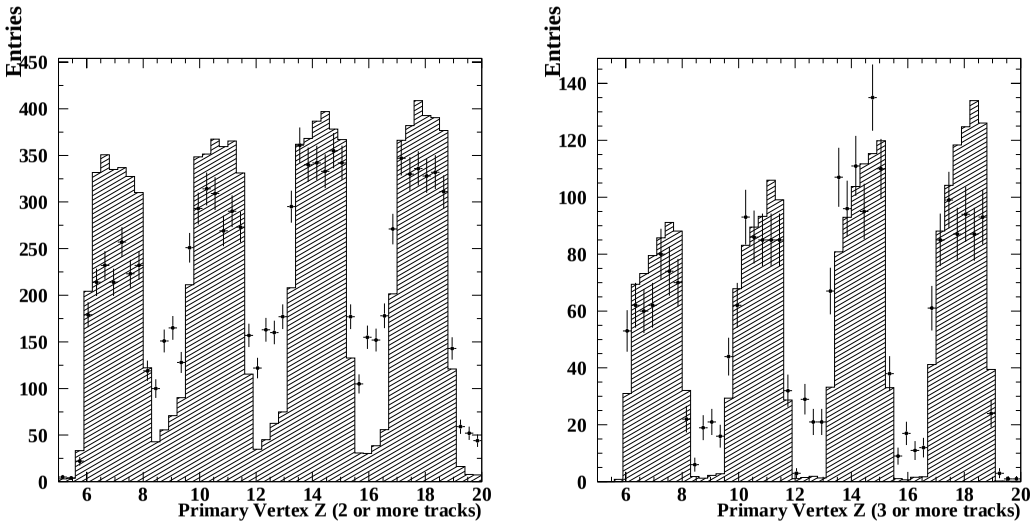

Figure 16: Distributions of the z position of primary vertex (cm). Left: only two or more tracks in the vertex. Right: three or more tracks in the vertex.

The Kalman vertex fit produces, through the square-root of the diagonal elements of the covariance matrix, an estimate of the uncertainty in the reconstructed vertex position in the y and z directions. These are shown in Fig. 17.

Fig. 18 shows the difference between the reconstructed primary vertex position and the true value as obtained from the Monte Carlo. Both distributions have been fitted to a Gaussian on top of a polynomial background and indicate a resolution from the central Gaussian of 19 μm in y and 78 μm

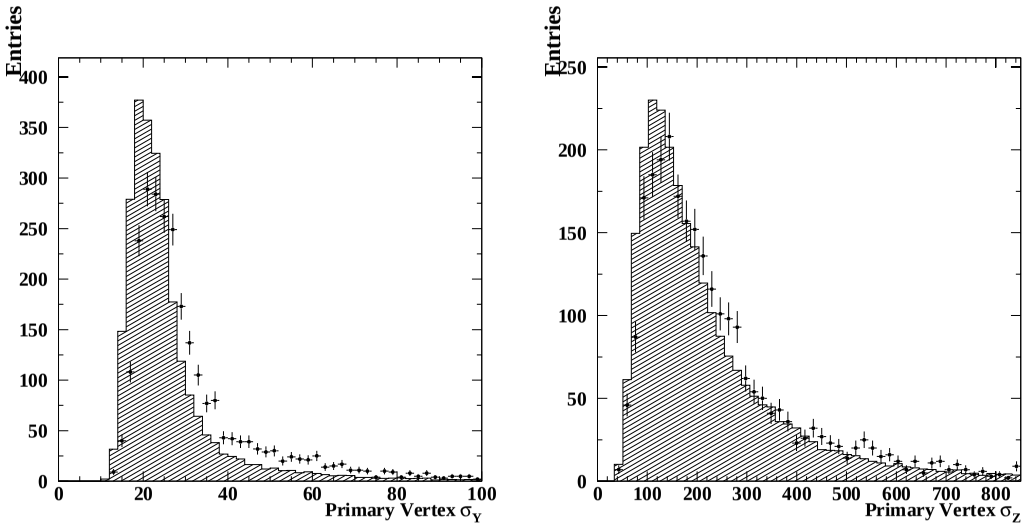

Figure 17: Distributions of the reconstructed uncertainties in the y (left) and z (right) position of the primary vertex (in μm).

in z. The resolution is better in the y direction due to the orientation of the strips and the fact that on average the tracks produced in the neutrino interaction tend to be produced at small angles to the z axis and thus constrain the z position by a smaller amount. The tails of the distributions are due to particles of low momenta and with low opening angle.

A test of the accuracy of the vertex reconstruction and error estimation can be obtained by plotting the "pull" of the variable V, which is the ratio:

$$Pull(V) = \frac{V_{reconstructed} - V_{MonteCarlo}}{\sigma_V}. \quad (1)$$

This variable should be normally distributed with a mean of 0 and a sigma of 1 (see Fig. 19). This demonstrates the accuracy of the error determination as obtained from the Kalman filter.

Fig. 20 shows a typical reconstructed ν_μ charged current interaction from the 1998 run.

7 Impact Parameter

As mentioned in section 1, the impact parameter signature is needed to identify ν_τ CC interactions, by the decay of the τ candidate, from the more numerous ν_μ CC background. We will describe in this section the final results of the impact parameter measurement of ν_μ CC interactions performed with NOMAD-STAR.

The vertex fit in NOMAD-STAR is used to obtain a measurement of the impact parameter resolution [36, 48]. In a ν_μ charged current interaction, the μ^- and hadronic jet come from the same point in space, and so if the μ^- track is removed from the vertex fit, it should still point at the vertex that is now composed only of the hadronic jet. The impact parameter is defined in this case as the projected signed distance onto the y-z plane of the μ^- from a ν_μ charged current interaction to the vertex produced by the remaining hadronic jet.

The procedure for measuring the impact parameter resolution of NOMAD–STAR uses both the Kalman vertex filter and its inverse filter [36]. The first stage is to fit the μ^- and hadronic jet into one vertex (the primary vertex). If there is an identified μ^- in the vertex, it can then be removed from the vertex using the inverse filter. At this point the vertex position is now determined only by the

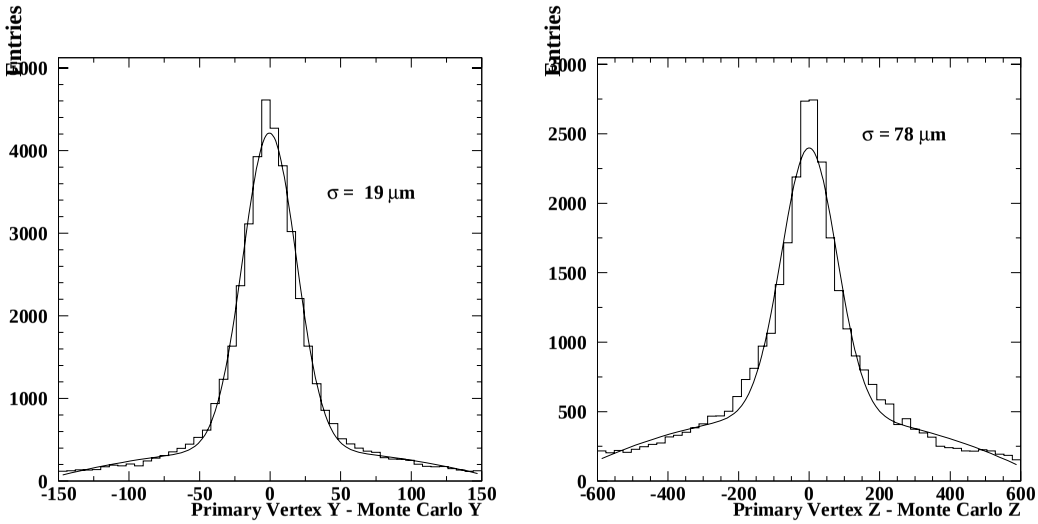

Figure 18: Distributions of the y (left) and z (right) position accuracy of the reconstructed primary vertex (in μm). The histograms are the data and the lines are fits to double Gaussians. The width of the central Gaussian is also shown.

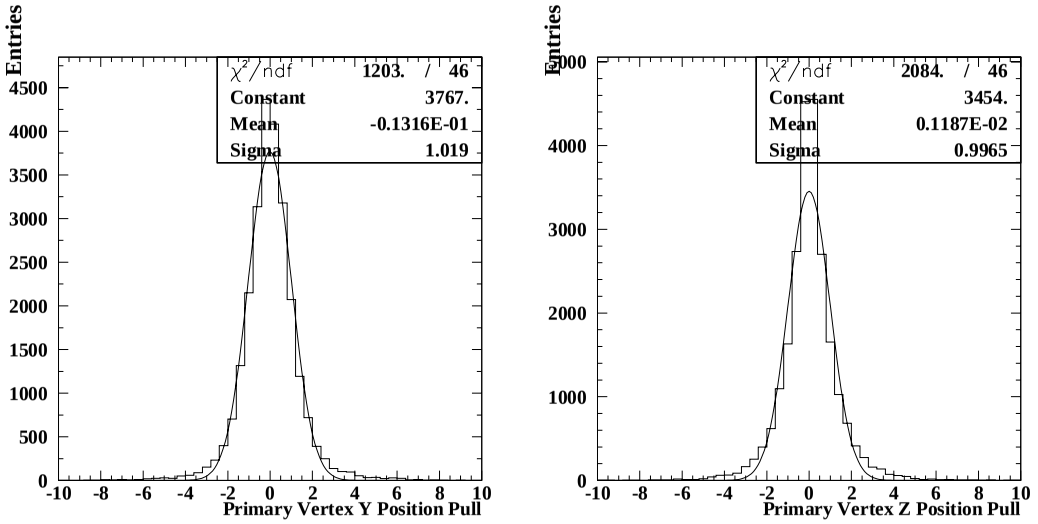

Figure 19: Distributions of the pulls on y (left) and z (right) primary vertex position. The histograms are the data and the lines are Gaussian fits. The width of the Gaussians are very close to 1.0.

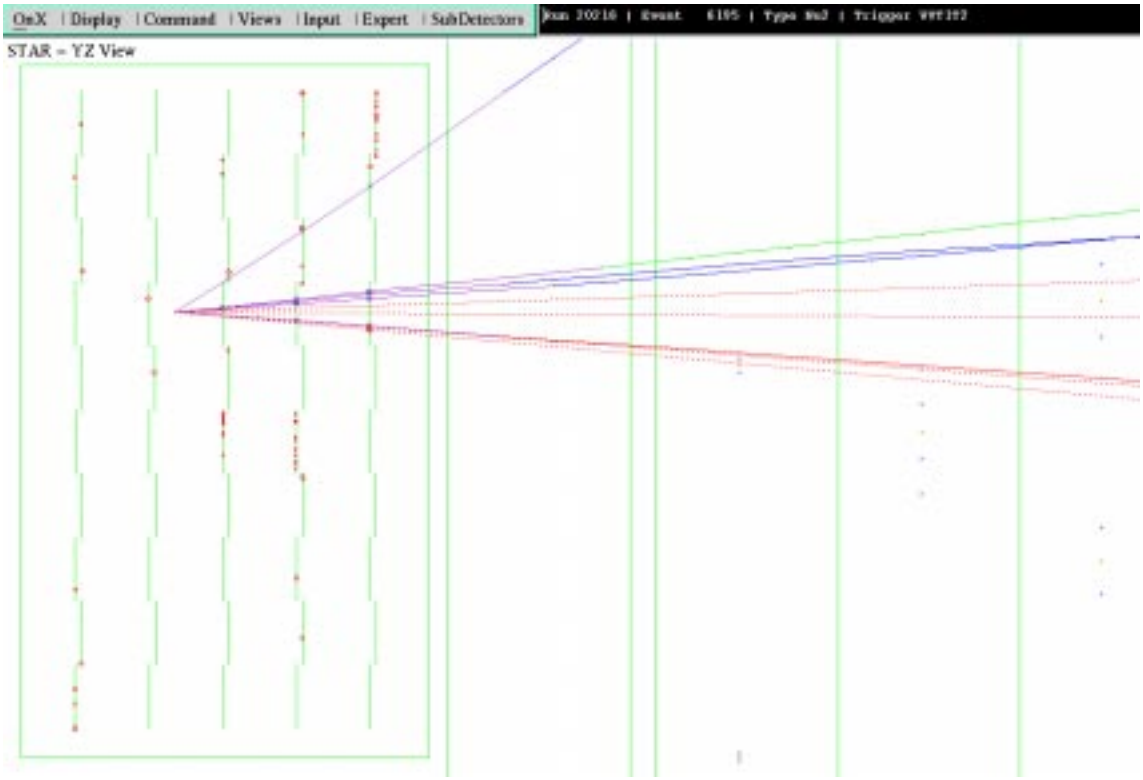

Figure 20: Reconstructed ν_μ charged current event from the 1998 run.

hadronic jet. The μ^- track can then be extrapolated to this new vertex position and the projected impact parameter can then be measured.

Preliminary results obtained for the impact parameter for the sample of the ν_μ charged current interactions obtained from the NOMAD-STAR 1998 data set were reported in [36, 48]. Using all events with more than two track primary vertices showed some non-Gaussian tails in the impact parameter significance distribution. Two track primary vertices with an opening angle in the y-z projection greater than 0.2 rad removed the non-Gaussian impact parameter significance tails and gave an impact parameter RMS of 36 μm [36].

Alternatively, if one includes only events with three tracks or more in the hadronic vertex (Fig. 21), the situation in which one has full three dimensional reconstruction is mimicked since it adds an extra track to the vertex fit of the hadronic jet. The final RMS on the impact parameter thus obtained is approximately 33 μm and the impact parameter significance plot (Fig. 21, right) shows a Gaussian shape with standard deviation of 1.00. This impact parameter RMS is similar to the value of 28 μm obtained in [23], in which this technique was studied to determine its efficiency for the detection of $\nu_\mu(\nu_e) \leftrightarrow \nu_\tau$ oscillations.

This study shows that the impact parameter resulting from the simulations of [23] closely matches (within 5 μm) that obtained from a real detector. One would then expect that the conclusions derived from that study would still be valid in a realistic situation. For a τ^- decaying to a μ^- one obtains an exponential impact parameter distribution with a RMS around 62 μm. According to [23], a detector of similar characteristics to NOMAD-STAR would have a 10% efficiciency for τ detection when the τ decays to one charged particle while having a background rejection factor of more than 10^6. The slightly larger impact parameter observed in NOMAD-STAR would affect these figures, but not by much.

The $\nu_\mu(\nu_e) \leftrightarrow \nu_\tau$ signature can be further mimicked in data by studying the decay of short

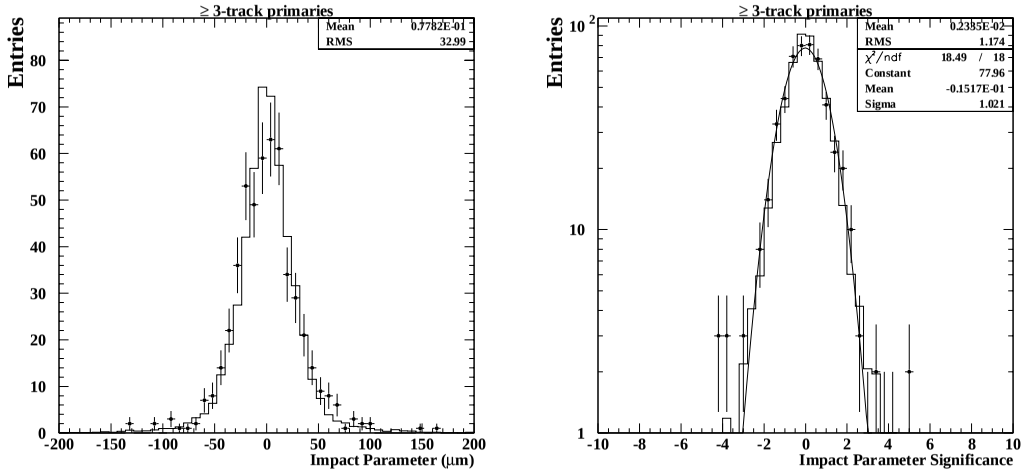

Figure 21: Impact parameter distribution (left) and impact parameter significance (right) of ν_μ CC data (points) and Monte Carlo (histogram) for all events with three or more tracks in the hadronic vertex.

lived particles like K^0_S and charm particles. The results from the short lived particle searches will be independently described in another publication [50] where the impact parameter and double vertex signatures are used to identify the signal.

8 Conclusion

The NOMAD-STAR detector was a silicon vertex detector installed in the NOMAD spectrometer at the CERN SPS neutrino beam. It consisted of four layers of a passive boron carbide target with a total mass of 45 kg and five layers of 600 single sided silicon microstrip detectors covering a total area of 1.14 m^2. About 11,500 ν_μ charged current interactions were reconstructed in the fiducial volume of NOMAD-STAR from the neutrino run in 1998.

The performance of the NOMAD–STAR detector has been described in this paper. The noise obtained from the 72 cm ladders was measured to be about 1500 e$^-$ (corresponding to a signal-to-noise ratio of about 17:1) and found to be stable for most ladders. Some other ladders were found to have a slowly varying noise that could exceed 2000 e$^-$ but these ladders were found to be still giving signal to noise of more than 12:1. The efficiencies of all the ladders were determined to be all above 92%, with some of the best ladders reaching efficiencies above 99%. Considering that these are the longest silicon ladders ever built, it shows that such long ladders can be used successfully for a large area silicon detector.

The track reconstruction residuals from the silicon detector was determined to have a RMS of 8.6 μm. The vertex resolution was found to be 19 μm in the y direction and 78 μm in the z direction, showing pull plots consistent with normalised Gaussians. Finally the projected impact parameter onto the y-z plane was found to have a value of 33 μm, demonstrating that such a detector could have the possibility of identifying τ decays by an impact parameter signature in a future $\nu_\mu(\nu_e) \leftrightarrow \nu_\tau$ experiment.

Acknowledgements We would like to thank all the people that have contributed to the NOMAD–STAR programme: J. Bensinger, A. Broksch, L. Dumps, J. Fuss, G. Gesuato, D. Geppert, S. Geppert, R. González, J.M. Jiménez, I. Krassine, K. Mühleman, J. Mulon, H. Noffke, I. Papadopoulos, J. Pin-

ney, C. Ricci, K. Rudolff, M. Smedbäck, M. Tareb, D. Voillat, A. Wellenstein and the encouragement and support of all the NOMAD institutions. F.J.P. Soler was supported by a TMR Fellowship from the European Commission. J. Kokkonen acknowledges support from the Helsinki Institute of Physics, the Academy of Finland, the Magnus Ehrnrooth Foundation, the Foundation for the Commercial and Technical Sciences (KAUTE), the Oskar Öflund Foundation and the Waldemar von Frenckell Foundation, all from Finland. Funding is also acknowledged from the ARC and DISR (Australia); EP Division (CERN); Institut National de Physique Nucléaire et Physique des Particules (IN2P3, France); Bundesministerium für Bildung und Forschung (Germany); Istituto Nazionale di Fisica Nucleare (INFN, Italy); Institute for Nuclear Research of the Russian Academy of Sciences (Russia); Fonds National Suisse de la Recherche Scientificque, Switzerland; Department of Energy (USA).

References

[1] Y. Fukuda et al., The Super Kamiokande Collaboration, Phys. Rev. Lett. 81 (1998) 1562-1567.

[2] T. Kajita, Nuclear Physics B (Proc. Suppl.) 77 (1999) 123-132.

[3] W.W.M.Allison et al., Soudan 2 Collaboration, Physics Letters B 449 (1999) 137-144.

[4] M.Ambrosio et al., MACRO Collaboration, Phys. Lett. B 517 (2001) 59-66.

[5] Q.R. Ahmad et al., SNO Collaboration, Phys. Rev. Lett. 87 (2001) 071301.

[6] Q.R. Ahmad et al., SNO Collaboration, Phys. Rev. Lett. 89 (2002) 011301.

[7] S. Fukuda et al., The Super Kamiokande Collaboration, Phys. Rev. Lett. 86 (2001) 5656-5660.

[8] W. Hampel et al., GALLEX-Collaboration, Phys. Lett. B 447 (1999) 127-133.

[9] J.N. Aburashitov et al., SAGE Collaboration, Phys. Rev. Lett. 83 (1999) 4686-4689.

[10] E. Bellotti, Nuclear Physics B (Proc. Suppl.) 91 (2001) 44-49.

[11] B. Cleveland et al., Astrop. J. 496 (1998) 505-526.

[12] V. Barger et al., Phys. Lett. B 537 (2002) 179-186.

[13] K. Nakamura, Nuclear Physics B (Proc. Suppl.) 91 (2001) 203-209.

[14] S.H. Ahn et al., Phys. Lett. B 511 (2001) 178-184.

[15] S.G. Wojcicki, Nuclear Physics B (Proc. Suppl.) 91 (2001) 216-222.

[16] A. Rubbia, Nuclear Physics B (Proc. Suppl.) 91 (2001) 223-229.

[17] A. Piepke, Nuclear Physics B (Proc. Suppl.) 91 (2001) 99-104.

[18] E.Eskut *et* al., CHORUS Collaboration, Nucl. Instr. and Meth. A401 (1997), 352.

[19] J. Altegoer *et al.*, The NOMAD Collaboration, Nucl. Instr. and Meth. A404 (1998) 96.

[20] E.Eskut *et* al., CHORUS Collaboration, Phys. Lett. B 497 (2001) 8-22.

[21] P. Astier *et al.*, The NOMAD Collaboration, Nucl. Phys. B 611 (2001) 3-39.

[22] A. de Santo, Int. J. Mod Phys. A 16 (2001) 4085-4151.

[23] J.J. Gómez-Cadenas, J.A. Hernando and A. Bueno, Nucl. Instr. and Meth. A378 (1996) 196.

[24] J.J. Gómez-Cadenas and J.A. Hernando, Nucl. Instr. and Meth. A381 (1996) 223-235.

[25] A.S. Ayan et al., CERN-SPSC/97-5,SPSC/I213, March , 1997.

[26] A Blondel et al., Nucl. Instr. and Meth. A 451 (2000) 102-122.

[27] R.Edgecock, W.J.Murray, J. Phys. G27 (2001) R141-R189.

[28] J.J. Gomez-Cadenas, D.A. Harris, Ann. Rev. Nucl. Part. Sci. 52 (2002) 253.

[29] M. Anfreville et al., Nucl. Instr. and Meth. A 481 (2002) 339-364.

[30] O. Toker, S. Masciocchi, E. Nygård, A. Rudge, P. Weilhammer, Nucl. Instr. and Meth. A340 (1994) 572.

[31] P.P. Allport *et al.*, Nucl. Instr. and Meth. A310 (1991) 155.

[32] G. Baricchello *et al.*, Nucl. Instr. and Meth. A413 (1998) 17-30.

[33] G. Baricchello *et al.*, Nucl. Instr. and Meth. A419 (1998) 1-15.

[34] GEANT 3.21, CERN Program Library Long Writeup W5013.

[35] A. Cervera-Villanueva, Nucl. Instr. and Meth. A 447 (2000) 100-109.

[36] A. Cervera-Villanueva *et al.*, Nucl. Instr. and Meth. A 486 (2002) 639-662.

[37] P. Astier et al., The NOMAD Collaboration, "Prediction of neutrino fluxes in the NOMAD experiment", Paper in preparation. To be submitted to Nucl. Instr. and Meth. A.

[38] M.C. Gonzalez-Garcia, J.J. Gomez-Cadenas, Phys. Rev. D 55 (1997) 1297.

[39] B. Van de Vyver, Nucl. Instr. and Meth. A 385 (1997) 91.

[40] G. Collazuol et al., Nucl. Instr. and Meth. A 449 (2000) 609, and references therein.

[41] G. Ambrosini et al., The SPY Collaboration, European Physical Journal C 10 (1999) 605-627.

[42] G. Ingelman, "LEPTO 6.1, the Lund Monte Carlo for deep inelastic lepton-nucleon scattering", In W. Buchmüller and G. Ingelman, editors, *Physics at HERA*, pages 1366-1394, Hamburg, 1992, DESY.

[43] T. Sjöstrand, "PYTHIA 5.7 and JETSET 7.4: Physics and Manual". Technical Report CERN-TH-7112/93, CERN, 1994.

[44] J. Altegoer *et al.*, Nucl. Instr. and Meth. A428 (1999) 299.

[45] V.E. Kuznetsov, Nucl. Phys. B (Proc. suppl.) 78 (1999) 287.

[46] J. Kokkonen, F.J.P. Soler, G. Vidal-Sitjes, "STAR Noise and Hit-finding Efficiency", Helsinki University of Technology Report HUT-F-A812 (2002), ISBN 951-22-5843-9, ISSN 1456-3320.

[47] J. Kokkonen, "A Silicon Detector for Neutrino Physics", Doctoral Thesis, Helsinki University of Technology, (2002), ISBN 951-45-8937-8, ISSN 1455-0563.

[48] F.J.P. Soler, Nucl. Instr. and Meth. A 477 (2002) 456-460.

[49] R. Frühwirth, Nucl. Instr. and Meth. A262 (1987) 444.

[50] P. Astier *et al.*, "Short lived particle identification capabilities of NOMAD-STAR." To be submitted for publication in Nucl. Instr. and Meth. A.